

Development and Flight Testing of a Parameter Identification Algorithm for Reconfigurable Control

David G. Ward,^{*} Jeffrey F. Monaco[†]

Barron Associates, Inc.

Marc Bodson[‡]

University of Utah

Abstract

The paper discusses the results of a series of flight tests in which a computationally efficient real-time parameter identification and control reconfiguration algorithm was evaluated. A modified sequential least-squares technique was used for identification. Significant challenges were encountered because of the poor information content of the signals used for identification and because of requirements for autonomy, reliability, and fast adaptation. A requirement for real-time operation in flight-control computers with limited computational throughput imposed additional constraints on the reconfigurable controller and the parameter estimation algorithm. The identification algorithm is presented in the paper with solutions that were developed to address problems posed by the specific application. Typical parameter identification results from the flight tests are shown.

^{*}D.G. Ward is Senior Research Scientist and Member AIAA. Barron Associates, Inc., The Jordan Building, 1160 Pepsi Place, Suite 300, Charlottesville, Virginia 22901.

[†]J.F. Monaco is Research Scientist. Barron Associates, Inc., The Jordan Building, 1160 Pepsi Place, Suite 300, Charlottesville, Virginia 22901.

[‡]M. Bodson is Associate Professor and Senior Member AIAA. Department of Electrical Engineering, University of Utah, Salt Lake City, Utah 84112.

The flight tests culminated in a successful landing of an F-16 with a simulated missing elevon.

Nomenclature

C_D	= drag coefficient
C_L	= lift coefficient
C_l	= rolling moment coefficient
C_m	= pitching moment coefficient
C_n	= yawing moment coefficient
C_T	= thrust coefficient
C_{Y_a}	= side force coefficient
D	= aerodynamic drag (along negative wind x axis), lb
I_{ii}	= vehicle body-axes moment of inertia, $slug - ft^2$
I_{ij}	= vehicle body-axes product of inertia, $slug - ft^2$
L	= aerodynamic lift (along negative wind z axis), lb
\bar{L}	= rolling moment, $ft - lb$
\bar{M}	= pitching moment, $ft - lb$
\bar{N}	= yawing moment, $ft - lb$
S	= wing reference area, ft^2
T_x	= vehicle thrust along body x axis, lb
V_t	= vehicle velocity, ft/sec
Y_a	= lateral force (along the wind y axis), lb
b	= vehicle wing span, ft
\bar{c}	= mean aerodynamic chord, ft

g_0	= constant gravitational acceleration in Earth z axis, ft/s^2
g_D	= component of gravitational acceleration along the wind x axis, ft/s^2
g_L	= component of gravitational acceleration along the wind z axis, ft/s^2
g_{Y_a}	= component of gravitational acceleration along the wind y axis, ft/s^2
m	= vehicle mass, <i>slug</i>
p	= body-axes roll rate, rad/s
q	= body-axes pitch rate, rad/s
\bar{q}	= free-stream dynamic pressure, lb/ft^2
r	= body-axes yaw rate, rad/s
x	= vector of vehicle states
y	= vector of measurements
α	= vehicle angle of attack, rad
β	= vehicle angle of sideslip, rad
δ_{fl}	= left trailing-edge flap (flaperon) deflection, rad
δ_{fr}	= right trailing-edge flap (flaperon) deflection, rad
δ_{lef}	= leading-edge flap deflection, rad
δ_{rud}	= rudder deflection, rad
δ_{tl}	= left tail (elevon) deflection, rad
δ_{tr}	= right tail (elevon) deflection, rad
γ	= vehicle flight path angle, rad
μ	= vehicle bank angle (about the velocity vector), rad
ρ	= air density, $slug/ft^3$
ϕ	= observation vector (regressor)
θ	= matrix of identified parameters

Introduction

A goal of modern flight control research is improved aircraft survivability and enhanced robustness of aircraft responses to a wide array of anomalous operating conditions. The emphasis on robustness has led to studies of reconfigurable control, which is intended to provide adaptation to imperfect characterizations of aircraft performance in new flight regimes, effector and airframe damage, and less traumatic events such as release of stores or gradual component aging. A notable milestone in the development of reconfigurable control systems was the flight testing of the so-called *Self-Repairing Flight Control System* that implemented a failure detection and identification approach to the problem [1]. An alternative to explicit failure detection is to provide reconfiguration via an adaptive control technique that does not require prior assumptions about the characteristics of failures.

During the summer of 1996, a series of flight tests demonstrated an adaptive approach to reconfigurable flight control called the *Self-Designing Controller* (SDC). This indirect adaptive control architecture computed a time-varying model of the aircraft dynamics and communicated the information to a receding-horizon control module. Using the identified dynamics, the controller calculated the effector commands required to achieve the desired aircraft responses as specified by a set of flying-qualities models. The SDC was shown to reconfigure rapidly to single and multiple impairments using residual effector authority. At the core of the algorithm was a novel on-line system identification technique that could rapidly track time-varying parameters and that was robust to adverse conditions of low excitation and correlated inputs. This paper presents the algorithm and the results of its implementation in flight tests.

Parameter identification of aircraft dynamics has long been a subject of interest in the aerospace community (see, *e.g.*, [2], [3], [4]). Problems such as identification of nonlinear dynamics [5] and reliable error analysis [6] continue to make it an area of active research today. The problem of parameter identification for reconfigurable flight control is similar, but brings additional difficulties, which may be categorized as follows:

- *Lack of control over the actuator signals.* A significant difficulty arises when the actuator signals are determined by a control law and cannot be freely selected. It has been shown that considerable improvements in identification performance can be obtained through optimization of the signals applied to the control surfaces [7]. Conversely, in a reconfigurable control application, the signals exhibit highly undesirable characteristics, including:

1. high levels of correlation between control signals and aircraft states (particularly for linear state-feedback control laws);
2. long periods of quiescence (*e.g.*, in steady flight); and
3. highly coupled longitudinal, lateral, and directional motions (especially for rapid roll maneuvers);

Because the control signals are determined by a control law which relies on the identification results, adverse interactions can also be introduced between the identification and the control components of the system.

- *Increased number of relevant parameters for failed aircraft.* Aircraft often lose their symmetry after failures, requiring that more parameters be identified. For example, the roll effectiveness of a symmetric tail deflection can be assumed to be zero for an unfailed aircraft but not for many post-failure scenarios.
- *Real-time operation.* The computational requirements of a parameter identification scheme for reconfigurable control must be compatible with available resources.
- *Automated Operation.* The on-line estimation procedure must be performed with minimal supervision and must not require extensive trial-and-error adjustments by the pilot.

In summary, the problem of identifying aircraft parameters poses considerable challenges when real-time operation under feedback control is required.

Equations of Motion and Parameterization for Identification

Equations of Motion

This section considers the nonlinear equations of motion of an aircraft. For this work, the authors followed the ANSI/AIAA recommended practice of using wind-axes force balances [8]. This yields the following nonlinear equations of motion

$$\dot{V}_t = \frac{1}{m} (T_x \cos \alpha \cos \beta - D) + g_D \quad (1)$$

$$\dot{\beta} = \frac{1}{mV_t} (Y_a - T_x \cos \alpha \sin \beta) + p \sin \alpha - r \cos \alpha + \frac{g_{Y_a}}{V_t} \quad (2)$$

$$\dot{\alpha} = -\frac{1}{mV_t \cos \beta} (L + T_x \sin \alpha) + q - \tan \beta (p \cos \alpha + r \sin \alpha) + \frac{g_L}{V_t \cos \beta} \quad (3)$$

The components of the wind-axes gravitational acceleration are given by $g_D = -g_0 \sin \gamma$, $g_{Y_a} = g_0 \cos \gamma \sin \mu$, and $g_L = g_0 \cos \gamma \cos \mu$.

The angular equations of motion are resolved in the body (not wind) axes system and are given by

$$\Gamma \dot{p} = I_{zz} \bar{L} + I_{xz} \bar{N} + I_{xz} (I_{xx} - I_{yy} + I_{zz}) pq + (I_{zz} (I_{yy} - I_{zz}) - I_{xz}^2) qr \quad (4)$$

$$I_{yy} \dot{q} = \bar{M} + (I_{zz} - I_{xx}) pr + I_{xz} (r^2 - p^2) \quad (5)$$

$$\Gamma \dot{r} = I_{xz} \bar{L} + I_{xx} \bar{N} + (I_{xx} (I_{xx} - I_{yy}) + I_{xz}^2) pq - I_{xz} (I_{xx} - I_{yy} + I_{zz}) qr \quad (6)$$

where $\Gamma = I_{xx} I_{zz} - I_{xz}^2$. It is assumed that I_{xy} and I_{yz} are identically zero, which may not always be valid for reconfigurable flight control of damaged aircraft.

The forces and moments acting on the aircraft are functions of the aerodynamic angles, α and β , of the body-axes angular rates, p , q , and r , and of the effector positions. For the F-16 aircraft used in the flight tests, the effectors are left and right tail (elevon), left and right trailing-edge flap (flaperon), and the rudder. The following effectors and pseudo-effectors were available to the reconfigurable control system

$$\delta_{ts} = \text{symmetric tail} = \frac{1}{2} (\delta_{tr} + \delta_{tl}) \quad (7)$$

$$\delta_{ta} = \text{asymmetric tail} = \frac{1}{2} (\delta_{tr} - \delta_{tl}) \quad (8)$$

$$\delta_{fa} = \text{asymmetric flaperon} = \frac{1}{2}(\delta_{fr} - \delta_{fl}) \quad (9)$$

$$\delta_{rud} = \text{rudder} \quad (10)$$

Pseudo-effectors were used because they allow one to incorporate parameter constraints in the identification algorithm that do not exist when one uses an effector suite comprised entirely of physical control surfaces.

Parameterization for Identification

For identification, it is necessary to represent the uncertain forces and moments of the equations of motions in terms of the parameters to be determined. While one may choose to identify nondimensional stability and control derivatives, it was preferable to identify dimensionalized coefficients. Relationships between the dimensional coefficients and standard, nondimensional derivatives are given in the Appendix. Although the dimensional parameters vary with Mach number and dynamic pressure, the variations are slow relative to those of the states, and the computations were found to be simplified in this manner.

The equations of motion are separated into longitudinal and lateral equations for identification purposes

$$\dot{x}_{lon} - NL_{lon}(p, q, r, \alpha, \beta) = \theta_{lon}^T \phi_{lon} \quad (11)$$

$$\dot{x}_{lat} - NL_{lat}(p, q, r, \alpha, \beta) = \theta_{lat}^T \phi_{lat} \quad (12)$$

where $x_{lon}^T = [q, \alpha]$ and $x_{lat}^T = [p, r, \beta]$. $NL_{lon}(p, q, r, \alpha, \beta)$ and $NL_{lat}(p, q, r, \alpha, \beta)$ represent the nonlinear terms due to inertial cross-couplings and orientation-dependent gravitational effects, and are given by

$$NL_{lon}(p, q, r, \alpha, \beta) = \begin{bmatrix} NL_q \\ NL_\alpha \end{bmatrix} = \begin{bmatrix} \frac{(I_{zz} - I_{xx})}{I_{yy}} pr + \frac{I_{xz}}{I_{yy}} (r^2 - p^2) \\ q - \tan \beta (p \cos \alpha + r \sin \alpha) + \frac{g_L}{V_t \cos \beta} \end{bmatrix} \quad (13)$$

$$NL_{lat}(p, q, r, \alpha, \beta) = \begin{bmatrix} NL_p \\ NL_r \\ NL_\beta \end{bmatrix} = \begin{bmatrix} \frac{I_{xz}(I_{xx} - I_{yy} + I_{zz})}{\Gamma} pq + \frac{(I_{zz}(I_{yy} - I_{zz}) - I_{xz}^2)}{\Gamma} qr \\ \frac{(I_{xx}(I_{xx} - I_{yy}) + I_{xz}^2)}{\Gamma} pq - \frac{I_{xz}(I_{xx} - I_{yy} + I_{zz})}{\Gamma} qr \\ p \sin \alpha - r \cos \alpha + \frac{g_{Y_a}}{V_t} \end{bmatrix} \quad (14)$$

ϕ_{lon} and ϕ_{lat} are vectors of observations (*regressors*), each consisting of aircraft states, effector positions, and a bias term

$$\phi_{lon}^T = [q, \alpha, \delta_{ts}, \delta_{ta}, 1], \quad \phi_{lat}^T = [p, r, \beta, \delta_{ts}, \delta_{ta}, \delta_{fa}, \delta_{rud}, 1] \quad (15)$$

and θ_{lon} , θ_{lat} are matrices of parameters to be identified

$$\theta_{lon}^T = \begin{bmatrix} \theta_q^T \\ \theta_\alpha^T \end{bmatrix} = \begin{bmatrix} \theta_{q_q} & \theta_{q_\alpha} & \theta_{q_{ts}} & \theta_{q_{ta}} & \theta_{q_0} \\ \theta_{\alpha_q} & \theta_{\alpha_\alpha} & \theta_{\alpha_{ts}} & \theta_{\alpha_{ta}} & \theta_{\alpha_0} \end{bmatrix} \quad (16)$$

$$\theta_{lat}^T = \begin{bmatrix} \theta_p^T \\ \theta_r^T \\ \theta_\beta^T \end{bmatrix} = \begin{bmatrix} \theta_{p_p} & \theta_{p_r} & \theta_{p_\beta} & \theta_{p_{ts}} & \theta_{p_{ta}} & \theta_{p_{fa}} & \theta_{p_{rud}} & \theta_{p_0} \\ \theta_{r_p} & \theta_{r_r} & \theta_{r_\beta} & \theta_{r_{ts}} & \theta_{r_{ta}} & \theta_{r_{fa}} & \theta_{r_{rud}} & \theta_{r_0} \\ \theta_{\beta_p} & \theta_{\beta_r} & \theta_{\beta_\beta} & \theta_{\beta_{ts}} & \theta_{\beta_{ta}} & \theta_{\beta_{fa}} & \theta_{\beta_{rud}} & \theta_{\beta_0} \end{bmatrix} \quad (17)$$

Regarding the parameterization, several issues are worth pointing out:

- Although the equations of motion are separated into longitudinal and lateral equations, the longitudinal and lateral variables appear in both equations, and the formulation does not constitute an assumption of separate longitudinal and lateral dynamics.
- The last parameter in each row of the parameter matrices is a bias term that includes the forces or moments not accounted for in the other parameters. These include trim-related variables of the aircraft and the unmodeled effects, including those related to Mach number and the slower-varying states.
- The equations are *linearly parameterized*, meaning that the unknown parameters appear linearly in the equations. This enables the use of efficient least-squares algorithms. One can represent nonlinear variations with respect to angle of attack by including terms such as α^2 , α^3 , etc. in the regressor vectors.
- For control purposes, the nonlinear (*NL*) portions of the equations of motion given in (13), (14) can be analytically linearized to obtain a linear state-space model. Note that the result is a set of equations with coupled longitudinal and lateral/directional dynamics.

- Nonlinear kinematics and gravitational terms are accounted for explicitly because these terms may vary rapidly with time (as rapidly as the states vary), and because their contributions are sometimes significant. Figs. 1 and 2 show the relative importance of two nonlinear effects observed from flight test data. The first plot shows \dot{q} as a dashed curve, and $pr(I_{zz} - I_{xx})/I_{yy} + (r^2 - p^2)I_{xz}/I_{yy}$ as a solid curve. The second plot shows $\dot{\alpha} - q$ as a dashed curve, and $\tan \beta(p \cos \alpha + r \sin \alpha)$ as a solid curve. The step-like variations in these curves are artifacts of the output rate of the flight-data recorder. Both cases represent maneuvers that are not particularly aggressive; nonetheless, the nonlinear effects account for visibly significant portions of the signals for long periods of time.
- Finally, an option would have been to identify terms such as $(I_{zz} - I_{xx})/I_{yy}$ in the algorithm. Although the inertia terms vary significantly with loading and configuration, it was found that the relative ratios were reasonably constant, and nominal values were used to reduce the number of parameters.

Regularized Parameter Identification Algorithm

The Modified Sequential Least Squares Algorithm

In the previous section, the equations of motion were cast in the form

$$y = \theta^{*T} \phi \tag{18}$$

Each column of θ contains the parameters corresponding to one component of the vector y .

There are two significant difficulties with the on-line estimation of the aircraft parameters, namely data collinearities and time-varying parameters. Data collinearities occur when any of the variables of the vector ϕ can be represented as linear combinations of the other variables. In such cases, the contributions of the components of θ^* may not be determined uniquely. Such a condition can be caused by: (1) trim flight conditions where surface and state commands are constant, (2) constant linear state feedback where the effector commands

are linear combinations of the states, or (3) “ganged” effectors (*e.g.*, linear combination of asymmetric flap and asymmetric tail to generate rolling moment). These collinearities are all examples of *insufficient excitation* and may lead to parameter divergence in an adaptive algorithm and in the presence of noise. A solution to the problem consists of extending the effective *memory* of the algorithm over periods of time that are long enough to ensure sufficient information is available.

Time-varying parameters result from changes in flight condition (slow variations) or during impairment, stores release, or other abrupt changes (fast variations). The presence of time-varying parameters translates into a need for rapid adaptation and, therefore, the need for short memory length. However, this requirement contradicts the need of *stretching* the algorithm memory long enough to obtain uncorrelated data.

To overcome the problem of identifying time-varying parameters in a system which is often insufficiently excited, a *modified sequential least-squares* (MSLS) algorithm was developed [9]. The parameter identification algorithm incorporates constraints to prevent numerical difficulties that can occur when data windows are small enough to track rapidly varying parameters. Constraints are added to a standard squared-error cost function with *forgetting*, to yield

$$J(\theta(t)) = \frac{1}{2} \sum_{k=t_0}^t \lambda^{t-k} \|y(k) - \theta(t)^T \phi(k)\|^2 + \frac{\nu}{2} \|W_0^{1/2} (K(t) - M\theta(t))\|^2 \quad (19)$$

where $y \in \mathfrak{R}^{o \times 1}$, $\phi \in \mathfrak{R}^{n \times 1}$ are vectors of measured signals, $\theta \in \mathfrak{R}^{n \times o}$ is a matrix of estimated parameters, n is the number of parameters per output y , and o is the number of signals in y . $\|\cdot\|$ is the Euclidean norm and $0.0 < \lambda \leq 1.0$ is the “forgetting factor” used to discount prior observations. The constraints consist of linear equalities of the form

$$K(t) = M\theta(t) \quad (20)$$

where $K(t) \in \mathfrak{R}^{\ell \times o}$ and $M \in \mathfrak{R}^{\ell \times n}$ define linear constraint relationships, with ℓ being the number of constraints. In (19) $W_0 \in \mathfrak{R}^{\ell \times \ell}$ is the matrix of relative penalties associated with each constraint, and $\nu \equiv \sum_{k=t_0}^t \lambda^{t-k}$ is the area of the window over which the cost function is

computed. (It is included in the penalty term so that the relative influence of a fixed weight remains the same, regardless of the value of the forgetting factor used.)

Temporal and *spatial* constraints are used. Temporal constraints penalize parameter values that deviate from their previous estimates. In such a case, $K(t) = \theta(t - dt)$, where $\theta(t - dt)$ is the estimate at the previous update, and $M \equiv I$ where $I \in \mathfrak{R}^{n \times n}$ is the identity matrix. Temporal constraints result in a smoothing over time, but do not hinder the ability to track rapidly varying parameters given sufficient excitation. Spatial constraints penalize parameter estimates that diverge from *a priori* estimates of their true values. These estimates can be constant, or they can be computed by on-board nonlinear models. Spatial constraints may also include constraints among the different parameters. For example, the lift and moment generated by a tail surface are related by the distance to the center of gravity, and this relationship may be incorporated as a constraint. Other constraints based on flight dynamics [10] may also be used.

Because the cost function in (19) is convex and continuously differentiable, its minimum can be found by solving $\frac{\partial J(\theta)}{\partial \theta} = 0$. From (19), it can be checked that

$$\frac{\partial J(\theta)}{\partial \theta} = \sum_{k=t_0}^t \lambda^{t-k} \phi(k) \phi^T(k) \theta + \nu M^T W_0 M \theta - \sum_{k=t_0}^t \lambda^{t-k} \phi(k) y^T(k) - \nu M^T W_0 K(t) \quad (21)$$

where $\frac{\partial J(\theta)}{\partial \theta}$ is a matrix whose i, j^{th} element is the derivative of J with respect to θ_{ij} . Solving for θ , one obtains

$$\theta(t) = \left[\sum_{k=t_0}^t \lambda^{t-k} \phi(k) \phi^T(k) + \nu M^T W_0 M \right]^{-1} \left[\sum_{k=t_0}^t \lambda^{t-k} \phi(k) y(k) + \nu M^T W_0 K(t) \right] \quad (22)$$

Note that the second term in the matrix inverse originates from the constraints. Without this term, the matrix could come close to singularity under low excitation conditions, resulting in a high sensitivity to noise. The term may be adjusted to ensure invertibility, even in the presence of insufficient excitation. This prevention of singularities is known as *regularization* [11] and is the principle behind a number of successful batch and nonlinear biased regression techniques such as ridge regression [12], truncated singular-value decomposition [13], and the

Levenberg Marquardt algorithm [14, 15]. In contrast to typical regularization schemes, the algorithm (22) has an additional term not only in the matrix inverse on the left, but also in the matrix on the right. In [16], it was shown that this additional term provided further smoothing capabilities in the presence of noise.

Recursive and Sequential Implementations of the Modified Least Squares Algorithm

For application to reconfigurable control, an implementation of the MSLS algorithm is needed that progressively computes new estimates of the parameters based on the latest data available. For that purpose, the main difficulty is the calculation of the matrix inverse. Note that the size of the matrix inverse depends on the number of regressor variables (*i.e.*, the dimension of ϕ), but not on the number of output variables (*i.e.*, the dimension of y). In other words, there is a considerable computational advantage to having several output variables share the same regressor. This advantage was exploited in the selection of the parameterization in section 2.2.

In [16], a *recursive* implementation of the algorithm was proposed which was similar to that of the standard recursive least-squares (RLS) algorithm and avoided the need to invert the matrix at every time instant. Because of the constraints, an approximate update of the matrix inverse had to be implemented, but the approximation was found to be satisfactory in reconfigurable flight control simulations [17]. An alternative approach, called here the *sequential* approach, consists of calculating the matrix inverse at periodic time intervals. The resulting algorithm is called the *modified sequential least-squares algorithm* (MSLS). Specifically, (22) is rewritten as

$$\theta(t) = R'^{-1}(t)s'(t) \tag{23}$$

with $R'(t)$ and $s'(t)$ given

$$R(t) = \lambda R(t - dt) + \phi(t)\phi^T(t) \tag{24}$$

$$R'(t) = R(t) + \nu M^T W_0 M \tag{25}$$

$$s(t) = \lambda s(t - dt) + \phi(t)y(t) \quad (26)$$

$$s'(t) = s(t) + \nu M^T W_0 K(t) \quad (27)$$

R and s should be initialized at $R(0) = \epsilon I$, where ϵ is a small positive constant and $I \in \Re^{n \times n}$ is the identity matrix, and $s(0) = R(0)\theta(0)$, where $\theta(0)$ is an arbitrary vector of initial coefficients. To solve (23), it is useful to recognize that $R'(t)$ is a symmetric positive definite matrix (assuming a full rank matrix $M^T W_0 M$), and that it may, therefore, be decomposed into upper and lower triangular matrices via Cholesky factorization. The Cholesky decomposition yields

$$G(t)G^T(t)\theta(t) = s'(t) \quad \text{or} \quad G(t)H(t) = s'(t) \quad (28)$$

Forward elimination is used to solve (28) for $H(t)$. Given $H(t)$, back-substitution will produce $\theta(t)$ from

$$G^T(t)\theta(t) = H(t) \quad (29)$$

The computational requirements of the sequential algorithm were compared to those of the recursive algorithm and to those of a sequential algorithm based on a Givens-rotation implementation. The three algorithms (Cholesky, Givens, and Recursive) were evaluated on a variety of sample problems, simulation data, and flight data. The results of these algorithms were qualitatively similar, so that the selection was based on ease of implementation and computational efficiency. For a five-parameter identification problem (typical of a single state equation in the application under consideration), the recursive algorithm required approximately 255 multiplications, the Cholesky technique required approximately 330 multiplications, and the Givens approach required approximately 590 multiplications. The Cholesky method was chosen because it represented significant savings over the Givens approach and was only slightly more computationally demanding than the recursive approach. A major advantage of the sequential approach over the recursive implementation was that computational load could be adjusted by performing the matrix inverse at a time interval compatible with available resources.

Convergence Properties of the Algorithm

The convergence properties of the algorithm may be established as follows. If the assumed model of the system is valid, there exists a true parameter vector θ^* such that

$$y(k) = \phi^T(k)\theta^* \quad (30)$$

for all k . As a consequence, the parameter error at time t is given by

$$\theta(t) - \theta^* = \left[\sum_{k=t_0}^t \lambda^{t-k} \phi(k)\phi^T(k) + \nu M^T W_0 M \right]^{-1} \left[\nu M^T W_0 (K(t) - M\theta^*) \right]. \quad (31)$$

Assume that the constraints may be split into temporal and spatial components such that

$$K(t) = \begin{bmatrix} M_t \theta(t_0) \\ M_s \theta^* \end{bmatrix} = \begin{bmatrix} M_t & 0 \\ 0 & M_s \end{bmatrix} \begin{bmatrix} \theta(t_0) \\ \theta^* \end{bmatrix} \quad (32)$$

where M_t is related to the temporal constraint and M_s is related to the spatial constraint (the true parameter θ^* is assumed to satisfy the spatial constraint). Then,

$$\theta(t) - \theta^* = [R_1 + R_2]^{-1} R_2 \begin{bmatrix} \theta(t_0) - \theta^* \\ 0 \end{bmatrix} \quad (33)$$

where

$$R_1 = \sum_{k=t_0}^t \lambda^{t-k} \phi(k)\phi^T(k), \quad R_2 = \nu M^T W_0 M. \quad (34)$$

The matrix R_1 is symmetric positive semi-definite. It is positive definite if persistency of excitation conditions are satisfied. The matrix R_2 is symmetric positive definite. Therefore,

$$\|\theta(t) - \theta^*\| \leq \alpha \|\theta(t_0) - \theta^*\| \quad (35)$$

for some $\alpha \leq 1$. Further, $\alpha \ll 1$ if $R_2 \ll R_1$, *i.e.*, if there is sufficient excitation and ν is sufficiently small. In other words, the error at time t is known to be less than or equal to the error at time t_0 , and it is much less than the initial error if there is enough excitation. Although the parameter error would, in theory, be zero for $\nu = 0$, the constraint is added to reduce the sensitivity of the algorithm to noise.

Off-Line Parameter Identification Results

The identification algorithm was evaluated using *Lockheed Martin's* nonlinear 6DOF simulation of the F-16 and flight data provided by *Calspan*. First, exhaustive experiments were conducted using a batch form of the identification algorithm (LS). This algorithm is the same as the algorithm discussed in the previous section, but with $\lambda = 1$ and no constraints.

In Table 1, the derivatives provided by the trim and linearization procedure are compared to those obtained by the identification algorithm for high-fidelity simulation data and for flight test data with inputs designed for longitudinal parameter identification. The flight condition is Mach 0.78 and 20,000 *ft* altitude. From Table 1, batch LS parameter identification results are in good agreement with the simulation's trim and linearization estimates of the longitudinal stability and control derivatives. (The simulation trim and linearization data provide the "true" parameters, obtained from wind-tunnel tests, flight experiments, and other analyses.) The match between the simulation data and the flight data was also good, although there remained a difference in the parameter θ_{q_α} that could not be explained. The difference in the parameter θ_{q_0} is not significant, because any discrepancy in the zero reference line of the tail surfaces would translate into a change in the parameter θ_{q_0} equal to the angular difference multiplied by $\theta_{q_{ts}}$. In other words, the difference in θ_{q_0} could be attributed to a bias in the calibration of the control surfaces' position of only 3 – 4 *deg*.

Fig. 3 shows the estimates of $\theta_{q_{ts}}$ and $\theta_{q_{ta}}$ obtained using the RLS algorithm. The solid curves correspond to the RLS parameter estimates, and the dotted lines correspond to the "true" parameters. In Fig. 3, the RLS algorithm is seen to estimate $\theta_{q_{ts}}$ with reasonable accuracy. However, the estimate of $\theta_{q_{ta}}$ provided by RLS is in error. Because the flight data consisted of pitch-axis maneuvering, the asymmetric elevon deflection was negligible and there was insufficient information to distinguish this parameter from the bias term, θ_{q_0} .

Fig. 4 shows MSLS parameter identification results for the same flight data. As before, the solid curve corresponds to the parameter estimate, and the dotted line represents the "true" parameter. The dashed line is a *spatial* constraint. In Fig. 4, the MSLS estimate of

$\theta_{q_{ts}}$ is slightly smoother than the corresponding RLS estimate, although the two parameter estimates are qualitatively similar. The MSLS estimate of $\theta_{q_{ta}}$ is markedly improved over the corresponding RLS parameter. (Note the change in plot scale.) Despite the absence of appreciable asymmetric elevon activity, the MSLS estimate is stable and well-contained, because temporal and spatial constraints regularize $\theta_{q_{ta}}$ during periods of low excitation.

It could be argued that the constraint simply biases the parameter towards the true value, and that this value would not be known in general. However, a spatial constraint of equal weight was applied to the symmetric tail contribution to pitching moment. Yet, because there was sufficient symmetric elevon activity, MSLS ignored the spatial constraint and faithfully tracked the true parameter. In other words, the spatial constraint does not have to be equal to the true parameter for the identified parameter to converge correctly in the presence of sufficient excitation. It only helps to maintain the parameter to a reasonable value when there is not sufficient information to determine that parameter.

Flight Test Results

VISTA/F-16 Implementation

The *VISTA/F-16* aircraft is sketched in Fig. 5. The aircraft contains a *Variable Stability System* (VSS) implemented on three *Rolm Hawk/32* computers. Each of the Hawk/32 computers had approximately the throughput of an *Intel 80286* processor, so that limits on computational power were a major consideration. Approximately one third of the collective computer resources were available for SDC use. The self-designing control software was segmented so that its computations could be shared by the three Hawk computers. One of the Hawk computers was used for the parameter identification algorithm and, because of computational limitations, was updated at approximately 13 *Hz*.

For safety, the VISTA digital flight control computer has logic that continuously monitors the VSS-computed commands and reverts control to the primary F-16 control laws if VSS commands are deemed unsafe. The logic is known as the *Vehicle Integrity Monitor*

(VIM) and is responsible for ensuring that the VSS system does not violate any pre-specified flight envelope or structural safety limits. An important structural restriction prevents any actuator commands from putting twist on the fuselage when the velocity exceeds 275 knots. Because a typical reconfiguration scenario is one in which asymmetric flaperon is used to counteract rolling moments generated on an impaired tail surface, all the flight tests had to be limited to speeds less than 275 knots.

Measurements

The identification algorithm requires measurements of the state variables α , β , q , p , and r . As Fig. 5 shows, the VISTA F-16 aircraft is equipped with an AOA (angle of attack) cone, two AOS (angle of sideslip) cones, and rate gyros. Together, these sensors provide measurements of all the state variables.

The derivatives of the state variables are also needed for identification. In this application, it was advantageous to use accelerometer measurements to generate these signals. Referring again to Fig. 5, note that the aircraft is equipped with three accelerometer stations (one at the pilot, and two slightly above and below the center of gravity). From those linear accelerometer measurements, the three rotational accelerations were reconstructed using standard formulas and the knowledge of the distances between the linear accelerometer stations. Accelerometer noise had relatively little impact on the parameter identification algorithm, which performed the required smoothing.

The derivatives $\dot{\alpha}$ and $\dot{\beta}$ can also be reconstructed from acceleration measurements, referred to the center of gravity of the aircraft. In this application, complementary filters from the standard VSS software provided clean signals for $\dot{\alpha}$ and $\dot{\beta}$, and the signals were used for identification.

The values of the control signals are also required. The effector positions were provided by synchros connected to the actuators. Symmetric and asymmetric pseudo-effector positions were computed from the left and right positions.

Constraints and Supervisory Functions

The flight-tested identification algorithm incorporated constraints on the parameters. Temporal constraints encouraged the parameters to be near previous values. Spatial constraints included relationships derived from flight mechanics and *a priori* values. For the maneuvers flown in the flights tests, many of the A -matrix terms varied as simple functions of flight condition. Using high-fidelity simulation data, quadratic polynomial neural network (PNN) models were synthesized for the expected values of these A -matrix terms. The networks were implemented as spatial constraints in the MSLS algorithm.

Prior to the first flight, the forgetting factors, temporal constraint weights, and spatial constraint weights were determined by an analyst based on the closed-loop responses of hundreds of Monte-Carlo simulations. Prior to the final flight, a random optimization technique, similar to simulated annealing or evolutionary programming, was used to find optimal values for these parameters using data from the first four flights.

A variety of supervisory functions were considered for the parameter identification. These functions included: (1) abrupt change detection, (2) adaptive levels of active noise injection, (3) removal of parameters associated with poor excitation, (4) freezing of the parameter estimates during periods of insufficient excitation, and (5) clamping of the parameter values. Low levels of active noise injection worked well in simulation and pilot-in-the-loop experiments, but the levels required to condition the parameters in flight tests degraded the aircraft flying qualities. Because of the regularization terms included in the MSLS algorithm, active noise injection was not required to generate appropriate parameter estimates, even during periods of reduced pilot input. However, it may be possible to improve identification results further by using novel active noise injection techniques. Current research is focused on using control allocation schemes to introduce effector signals that are orthogonal to aircraft moment-generating capabilities, i.e., commanding time-varying combinations of effector displacements that enhance the information content of the identification process while simultaneously producing identical commanded aircraft motions.

Ultimately, the only supervisory function that was used in the SDC software was parameter clamping. This function was implemented as a precaution against unforeseen parameter divergence. The values at which the parameters were clamped were determined by considering a variety of conditions and obtaining the maximum and minimum values from simulation data. To account for failure situations, many parameter limits were further modified to allow greater variations that might be encountered under a wide variety of failure scenarios.

Failure Simulation

The software had a self-contained failure module. Single or multiple failures could be triggered at desired times. The failure module intercepted the control law commands, modified them, and sent the modified commands to the actuators. For 100% effective (unimpaired) surfaces, the actuator commands were not modified by the failure simulation, and for 0% effective control surfaces, an effector was commanded to “float” parallel to the local flow, thus approximating a missing surface. A partially missing actuator was commanded between the floating position and the desired displacement.

Ineffective left and right tail surfaces were simulated by commanding the corresponding surface to the negative of the local angle of attack. The local angle of attack is different from the aircraft angle of attack due to downwash effects at the tail. The downwash at the tail stems almost entirely from the trailing-edge vortex system of the wings. It reduces the effective angle of attack at the tail. Data for the F-16, provided by researchers at *Wright Laboratory*, showed that the downwash variation with aircraft angle of attack was approximately linear within the restricted flight envelope allowed by the vehicle integrity monitor, and this linear relationship was used for failure simulation.

Ineffective left or right flaperons were simulated by commanding the effectors to the negative of the aircraft angle of attack. Similarly, an ineffective rudder was simulated by commanding the rudder to the aircraft angle of sideslip. It is noted that a missing (or floating) surface will result in a reduction of aircraft stability and decreased effectiveness. This is not the case with locked-surface impairments.

Upon activation of a failure, effector positions were transitioned from their current values to those of the failed control surfaces over a period of several seconds. Ground simulation and flight test experiments led to a choice of a time constant such that the actual effectiveness was 50% of the desired value after 1 *sec.*, 75% after 2 *sec.*, 87.5% after 3 *sec.*, etc. While batch and piloted simulations indicated that the adaptive algorithm could readily compensate for abrupt (instantaneous) changes in effectiveness, the transition was required so that actuators were not driven at their rate limits and so that safety (VIM) constraints were not violated.

In addition to modifying the actuator commands, the failure simulation computed the difference between the commanded positions sent to the failure simulation and those sent to the actuators. The information was added to the signals that were communicated to the parameter identification algorithm so that the estimator would believe that the effectors achieved their commanded deflections. This simple adjustment was adequate because the actuator dynamics were fast and close to linear.

Parameter Identification Results

The *self-designing controller* (SDC) underwent flight testing during the period from May 14, 1996, to July 9, 1996. Five test flights were performed, each lasting approximately one hour. The test plan for the first flight called for the entire control algorithm and associated software to be engaged; then, depending on the results, experiments of increasing or decreasing difficulty would be tried. This kind of approach was possible because of the safety provided by the VISTA F-16 Vehicle Integrity Monitor module.

Because the flight tests included the evaluation of the reconfigurable control law, considerable effort was spent adjusting the desired control responses for flying qualities. The remaining time was spent addressing and resolving problems with the parameter identification. Few such problems were encountered, but during one of the flights, there was a divergent nose-down transient exhibited by the SDC. Post-flight analysis revealed that the pitch excursion resulted from a zero-valued estimate for the contribution of the symmetric elevon to pitch acceleration. Inspection and analysis of the data revealed that the problem

was due to small errors in the inertial cross-coupling compensation, which were manifested during multi-axes maneuvers where the cross-couplings were significant. The pitch rate equation was the most susceptible to these problems because of large roll and yaw rates attained for relatively mild turns (recall Figs. 1 and 2).

To remedy the problem, the forgetting factors, temporal weighting matrices, and spatial weighting matrices were optimized to avoid temporary excursions of the parameters to undesirable values. The settings were obtained off-line using a guided-random search algorithm and were chosen to minimize the weighted-sum-squared error between key estimates obtained on flight-test data and “true ” parameters obtained via high-fidelity simulations.

Parameter identification results, using the optimal settings, are shown in Fig. 6. The solid curves show the estimated parameters and the dashed curves show the “true” parameters (the quotes refer to the fact that the true parameters are only estimates of the parameters based on wind-tunnel data and other analyses). The progressive engagement of the failure is visible from the responses, and the identified parameters are found to converge to the true parameters. Convergence of the asymmetric tail parameters is slower because of the lower level of activity in that signal. As expected, one finds that the pitching effectiveness of the symmetric tail deflection is halved after the failure. Also, the pitching effectiveness of the asymmetric deflection moves from zero to the same effectiveness as that of the symmetric deflection. An identical, but reversed picture, is observed for the rolling moment.

Fig. 7 shows the pitch rate and elevon commands during landing with a (simulated) missing left elevon. The plot on the top shows the pitch rate and the desired pitch rate specified by the flying-qualities model. The plot below shows the elevon positions. Time histories begin 35 sec. into the flight record, at the time of SDC engagement and failure activation. They terminate at touchdown approximately 150 sec. into the record. The figure shows that there were no significant transients upon activation of the impairment. The left elevon moved to a position equal to approximately one degree, and floated at the local angle of attack. The position of the right elevon moved in the opposite direction to maintain trim

of the aircraft, stabilize the aircraft, and achieve the desired pitch rate.

Despite the effects of a simulated failure being compounded by a significant crosswind (15 *kts.*) and gusty conditions during the landing, flying qualities were satisfactory for all axes, and, as noted by the flight crew, performance of the adaptive control law was consistent and predictable for the entire flight. To the authors' knowledge, this was the first time that an aircraft with simulated damage had been landed under reconfigurable control.

Conclusions

The identification of aircraft parameters for use in reconfigurable control poses significant challenges. The problems are largely due to the poor information content of the signals used for identification combined with the need for rapid adaptation. As a solution to this problem, this paper proposed a modified least-squares algorithm which incorporates temporal and spatial constraints. This novel on-line system identification technique was found to rapidly track time-varying parameters and to be robust to adverse conditions such as low excitation or correlated inputs. A significant part of the design was the selection of an appropriate model structure, which accounted for the nonlinear dynamics of importance with a minimal number of parameters. The choice of temporal and spatial constraints was also critical to the performance of the algorithm. A series of flight tests resulted in a landing under a simulated failure condition and on-line reconfigurable control, and demonstrated the success of the identification algorithm in determining the parameters of the aircraft in real-time.

Acknowledgments

This work was sponsored by the Directorate of Mathematical and Computer Sciences, Air Force Office of Scientific Research, Bolling AFB, DC, under SBIR Phase II Contract F49620-94-C-0087. The third author was also sponsored by the Air Force Office of Scientific Research, Air Force Materiel Command, USAF, under grant number F49620-95-1-0341.

References

- [1] Urnes, J., Yeager, R. and Stewart, J., "Flight Demonstration of the Self-Repairing Flight Control System in a NASA F-15 Aircraft," presented at *the National Aerospace Electronics Conference* (Dayton, OH), 1990.
- [2] Maine, R., and Murray, J., "Application of Parameter Estimation to Highly Unstable Aircraft," *Journal of Guidance, Control, and Dynamics*, Vol. 11, No. 3, 1988, pp. 213-219.
- [3] Iliff, K., "Parameter Estimation for Flight Vehicles," *Journal of Guidance, Control, and Dynamics*, Vol. 12, No. 5, 1989, pp. 609-622.
- [4] Tischler, M., "System Identification Methods for Aircraft Flight Control Development and Validation," in *Advances in Aircraft Flight Control*, M. Tischler ed., Taylor & Francis, Bristol, PA, 1996, pp. 35-69.
- [5] Trankle, T., and Bachner, S., "Identification of a Nonlinear Aerodynamic Model of the F-14 Aircraft," *Journal of Guidance, Control, and Dynamics*, Vol. 18, No. 6, 1995, pp. 1292-1297.
- [6] Morelli, E., and Klein, V., "Accuracy of Aerodynamic Model Parameters Estimated from Flight Test Data," *Journal of Guidance, Control, and Dynamics*, Vol. 20, No. 1, 1997, pp. 74-80.
- [7] Morelli, E., "Flight Test Validation of Optimal Input Design and Comparison to Conventional Inputs," *Proceedings of the Atmospheric Flight Mechanics Conference* (New Orleans, LA), 1997, pp. 573-583.
- [8] Anon., *Recommended Practice for Atmospheric and Space Flight Vehicle Coordinate Systems*, ANSI/AIAA Standard R-004-1992, American National Standard Institute, New York, NY, 1992.

- [9] Ward, D., and Barron, R., “A Self-Designing Receding Horizon Optimal Flight Controller,” *Proceedings of the American Control Conference* (Seattle, WA), 1995, pp. 3490-3494.
- [10] Chandler, P., Pachter, M., and Mears, M., “System Identification for Adaptive and Reconfigurable Control,” *Journal of Guidance, Control, and Dynamics*, Vol. 18, No. 3, 1995, pp. 516-524.
- [11] Söderström, T., and Stoica, P., *System Identification*, Prentice Hall, Englewood Cliffs, NJ, 1989.
- [12] Cherkassky, V., Friedman, J., and Wechsler, H., *From Statistics to Neural Networks, Theory and Pattern Recognition Applications*, Springer-Verlag, Berlin, 1993.
- [13] Van Huffel, S., and Vanderwalle, J., *The Total Least Squares Problem: Computational Aspects and Analysis*, SIAM, Philadelphia, PA, 1991.
- [14] Ljung, L., and Söderström, T., *Theory and Practice of Recursive Identification*, MIT Press, Cambridge, MA, 1983.
- [15] Seber, G., and Lee, C., *Advances in Neural Information Processing Systems*, Wiley and Sons, New York, NY, 1989.
- [16] Bodson, M., “An Adaptive Algorithm with Information-Dependent Data Forgetting,” *Proceedings of the American Control Conference* (Seattle, WA), 1995, pp. 3485-3489.
- [17] Bodson, M. and Groszkiewicz, J., “Multivariable Adaptive Algorithms for Reconfigurable Flight Control,” *IEEE Transactions on Control Systems Technology*, Vol. 5, No. 2, 1997, pp. 217-229.

Appendix: Relationship between the Parameters and the Dimensionless Derivatives

The forces and moments acting on the aircraft can be defined in terms of dimensionless aerodynamic coefficients, with: $T_x = \bar{q}SC_T$, $D = \bar{q}SC_D$, $Y_a = \bar{q}SC_{Y_a}$, $L = \bar{q}SC_L$, $\bar{L} = \bar{q}SbC_l$,

$\bar{M} = \bar{q}S\bar{c}C_m$, $\bar{N} = \bar{q}SbC_n$, where $\bar{q} = \frac{1}{2}\rho V_t^2$ is the free-stream dynamic pressure, S is the wing reference area, b is the wing span, and \bar{c} is the mean aerodynamic chord of the wing.

The dimensionless coefficients are parameterized as follows

$$C_m = C_{m_0} + C_{m_\alpha}\alpha + C_{m_{\dot{\alpha}}}\dot{\alpha} + C_{m_q}q + C_{m_{ts}}\delta_{ts} + C_{m_{ta}}\delta_{ta} \quad (36)$$

$$C_L = C_{L_0} + C_{L_\alpha}\alpha + C_{L_{ts}}\delta_{ts} + C_{L_{ta}}\delta_{ta} \quad (37)$$

$$C_l = C_{l_0} + C_{l_\beta}\beta + C_{l_p}p + C_{l_r}r + C_{l_{ts}}\delta_{ts} + C_{l_{ta}}\delta_{ta} + C_{l_{fa}}\delta_{fa} + C_{l_{rud}}\delta_{rud} \quad (38)$$

$$C_n = C_{n_0} + C_{n_\beta}\beta + C_{n_p}p + C_{n_r}r + C_{n_{rud}}\delta_{rud} \quad (39)$$

$$C_{Y_a} = C_{Y_0} + C_{Y_\beta}\beta + C_{Y_{rud}}\delta_{rud} \quad (40)$$

The dimensionless derivatives are related to the parameters in (16), (17) by the following equations

$$\begin{bmatrix} \theta_{q_q} \\ \theta_{q_\alpha} \\ \theta_{q_{ts}} \\ \theta_{q_{ta}} \\ \theta_{q_0} \end{bmatrix} = \frac{\bar{q}S\bar{c}}{I_{yy}} \begin{bmatrix} C_{m_q} \\ C_{m_\alpha} + C_{m_{\dot{\alpha}}}\theta_{\alpha\alpha} \\ C_{m_{ts}} + C_{m_{\dot{\alpha}}}\theta_{\alpha_{ts}} \\ C_{m_{ta}} + C_{m_{\dot{\alpha}}}\theta_{\alpha_{ta}} \\ C_{m_0} + C_{m_{\dot{\alpha}}}\theta_{\alpha_0} \end{bmatrix} \quad \begin{bmatrix} \theta_{\alpha_q} \\ \theta_{\alpha_\alpha} \\ \theta_{\alpha_{ts}} \\ \theta_{\alpha_{ta}} \\ \theta_{\alpha_0} \end{bmatrix} = -\frac{\bar{q}S}{mV_t \cos \beta} \begin{bmatrix} C_{L_q} (\approx 0.0) \\ C_{L_\alpha} + \frac{T_x \sin \alpha}{\bar{q}S} \\ C_{L_{ts}} \\ C_{L_{ta}} \\ C_{L_0} - \frac{mgL}{\bar{q}S} \end{bmatrix} \quad (41)$$

$$\begin{bmatrix} \theta_{p_p} \\ \theta_{p_r} \\ \theta_{p_\beta} \\ \theta_{p_{ts}} \\ \theta_{p_{ta}} \\ \theta_{p_{fa}} \\ \theta_{p_{rud}} \\ \theta_{p_0} \end{bmatrix} = \frac{\bar{q}Sb}{\Gamma} \begin{bmatrix} I_{zz}C_{l_p} + I_{xz}C_{n_p} \\ I_{zz}C_{l_r} + I_{xz}C_{n_r} \\ I_{zz}C_{l_\beta} + I_{xz}C_{n_\beta} \\ I_{zz}C_{l_{ts}} + I_{xz}C_{n_{ts}} \\ I_{zz}C_{l_{ta}} + I_{xz}C_{n_{ta}} \\ I_{zz}C_{l_{fa}} + I_{xz}C_{n_{fa}} \\ I_{zz}C_{l_{rud}} + I_{xz}C_{n_{rud}} \\ I_{zz}C_{l_0} + I_{xz}C_{n_0} \end{bmatrix} \quad \begin{bmatrix} \theta_{r_p} \\ \theta_{r_r} \\ \theta_{r_\beta} \\ \theta_{r_{ts}} \\ \theta_{r_{ta}} \\ \theta_{r_{fa}} \\ \theta_{r_{rud}} \\ \theta_{r_0} \end{bmatrix} = \frac{\bar{q}Sb}{\Gamma} \begin{bmatrix} I_{xx}C_{n_p} + I_{xz}C_{l_p} \\ I_{xx}C_{n_r} + I_{xz}C_{l_r} \\ I_{xx}C_{n_\beta} + I_{xz}C_{l_\beta} \\ I_{xx}C_{n_{ts}} + I_{xz}C_{l_{ts}} \\ I_{xx}C_{n_{ta}} + I_{xz}C_{l_{ta}} \\ I_{xx}C_{n_{fa}} + I_{xz}C_{l_{fa}} \\ I_{xx}C_{n_{rud}} + I_{xz}C_{l_{rud}} \\ I_{xx}C_{n_0} + I_{xz}C_{l_0} \end{bmatrix} \quad (42)$$

$$\begin{bmatrix} \theta_{\beta_p} \\ \theta_{\beta_r} \\ \theta_{\beta_\beta} \\ \theta_{\beta_{ts}} \\ \theta_{\beta_{ta}} \\ \theta_{\beta_{fa}} \\ \theta_{\beta_{rud}} \\ \theta_{\beta_0} \end{bmatrix} = \frac{\bar{q}S}{mV_t} \begin{bmatrix} C_{Y_p} (\approx 0.0) \\ C_{Y_r} (\approx 0.0) \\ C_{Y_\beta} - \frac{T_x}{\bar{q}S} \cos \alpha \frac{\sin \beta}{\beta} \\ C_{Y_{ts}} (\approx 0.0) \\ C_{Y_{ta}} (\approx 0.0) \\ C_{Y_{fa}} (\approx 0.0) \\ C_{Y_{rud}} \\ C_{Y_0} + \frac{mg_{y0}}{\bar{q}S} \end{bmatrix} \quad (43)$$

Some parameters are typically small, as indicated in the vectors. However, to share computations among the different variables of the longitudinal and lateral channels, all of the coefficients were identified.

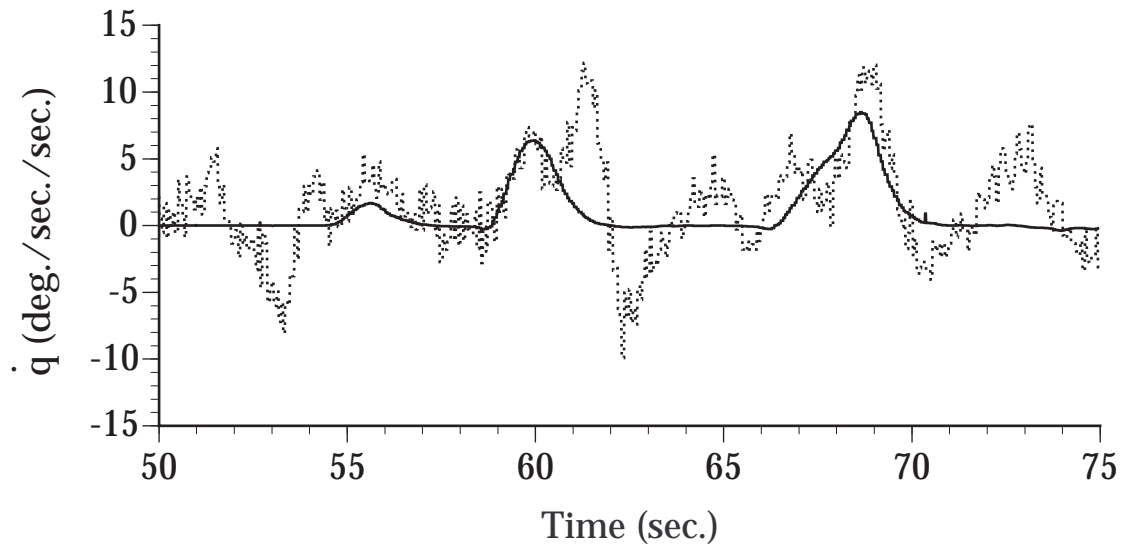


Figure 1: Contribution of Nonlinear Effects to the \dot{q} Response

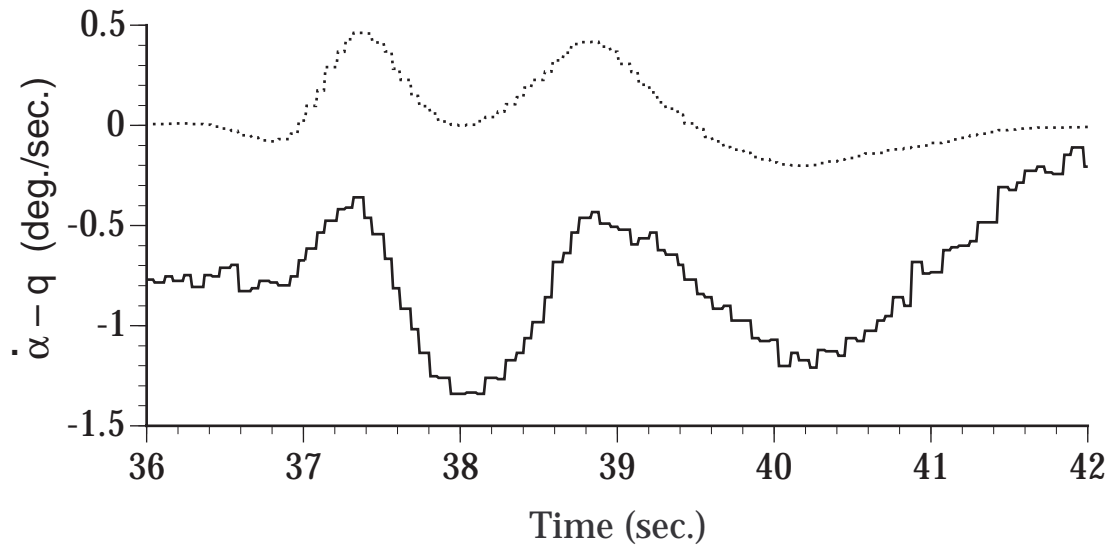


Figure 2: Contribution of Nonlinear Effects to the $\dot{\alpha}$ Response

Table 1: Longitudinal Stability and Control Derivatives

Parameter	Trim & Linearize (Sim. Truth)	Batch LS (Sim. Data)	Batch LS (Flight Data)
θ_{q_q} (1/sec.)	-0.64	-0.43	-0.42
θ_{q_α} (1/sec./sec.)	-1.62	-1.91	-3.09
$\theta_{q_{ts}}$ (1/sec./sec.)	-14.3	-14.0	-12.6
θ_{q_0} (rad./sec./sec.)	-23.6	-22.2	18.7
θ_{α_q} (—)	0.99	1.00	0.99
θ_{α_α} (1/sec.)	-0.91	-0.91	-0.88
$\theta_{\alpha_{ts}}$ (1/sec.)	-0.14	-0.14	-0.13
θ_{α_0} (rad./sec.)	2.08	2.09	2.55

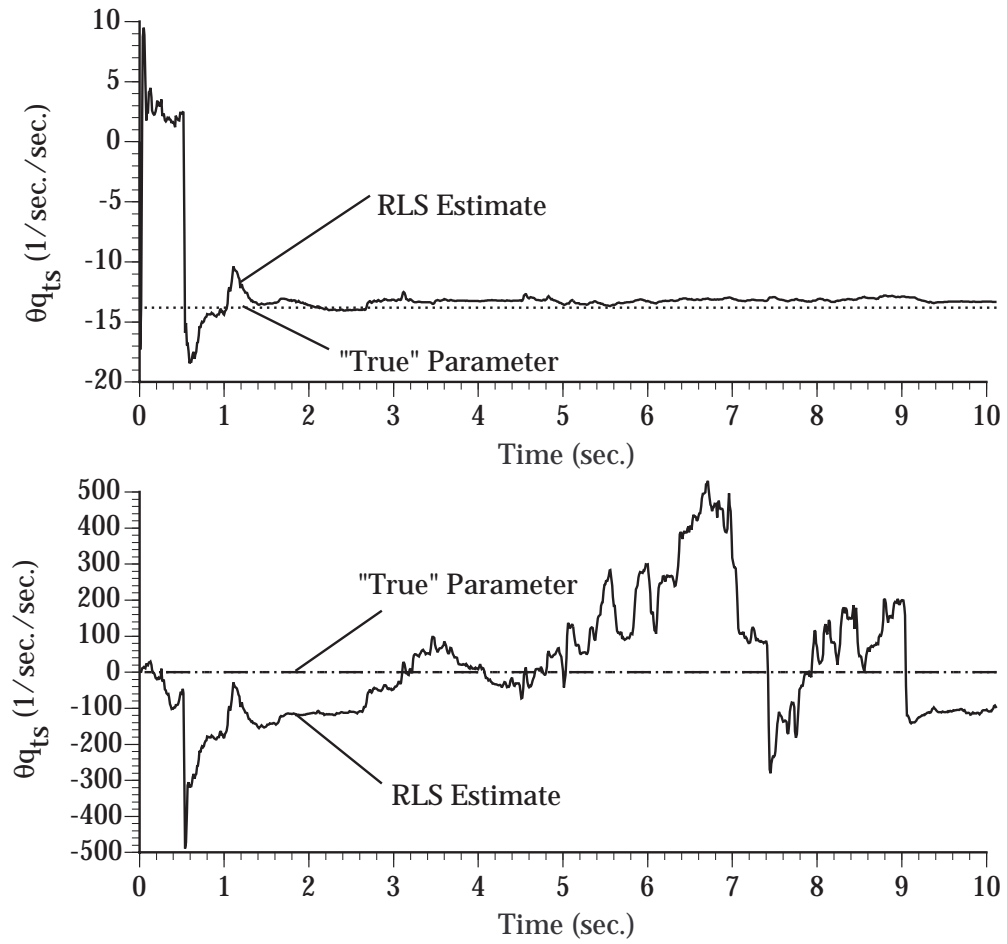


Figure 3: RLS Estimates of $\theta_{q_{ts}}$ and $\theta_{q_{ta}}$

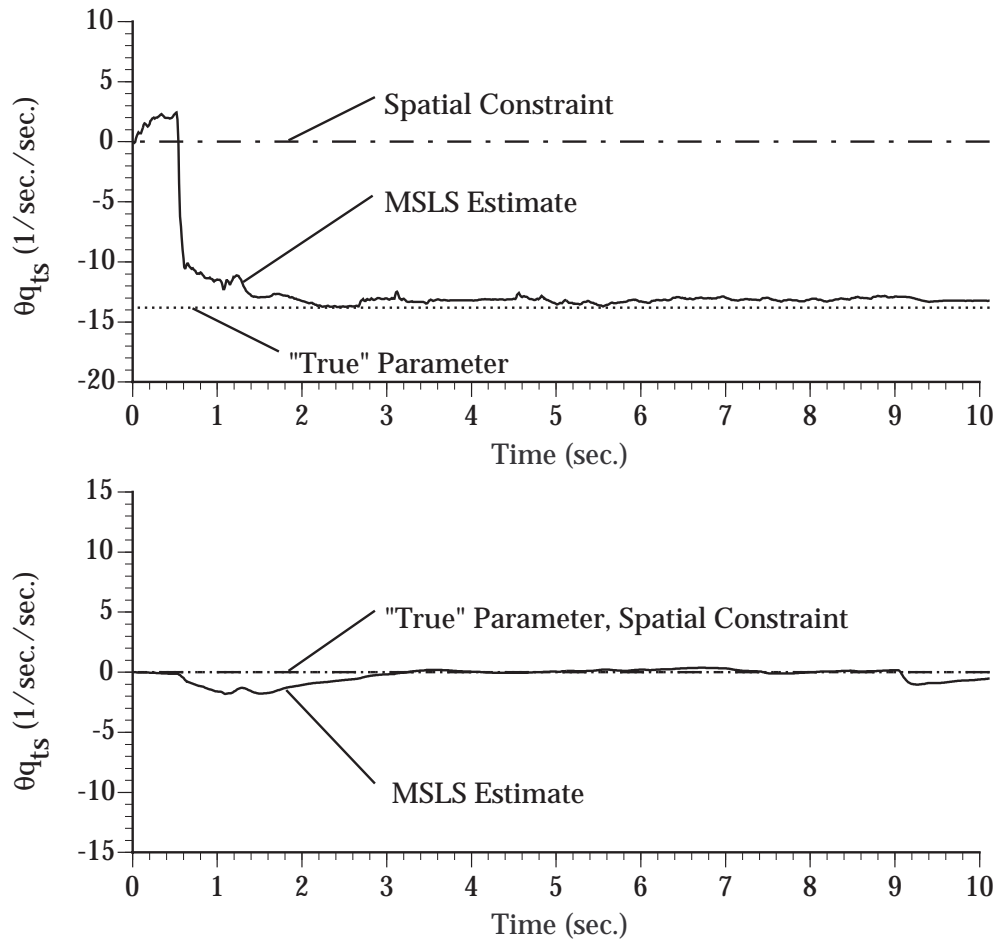


Figure 4: MSLS Estimates of $\theta_{q_{ts}}$ and $\theta_{q_{ta}}$

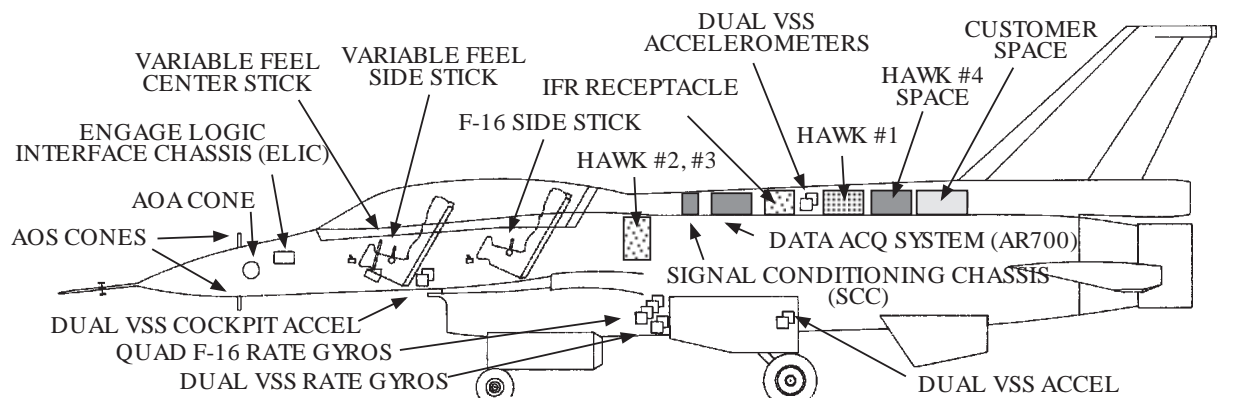


Figure 5: VISTA F-16 Aircraft

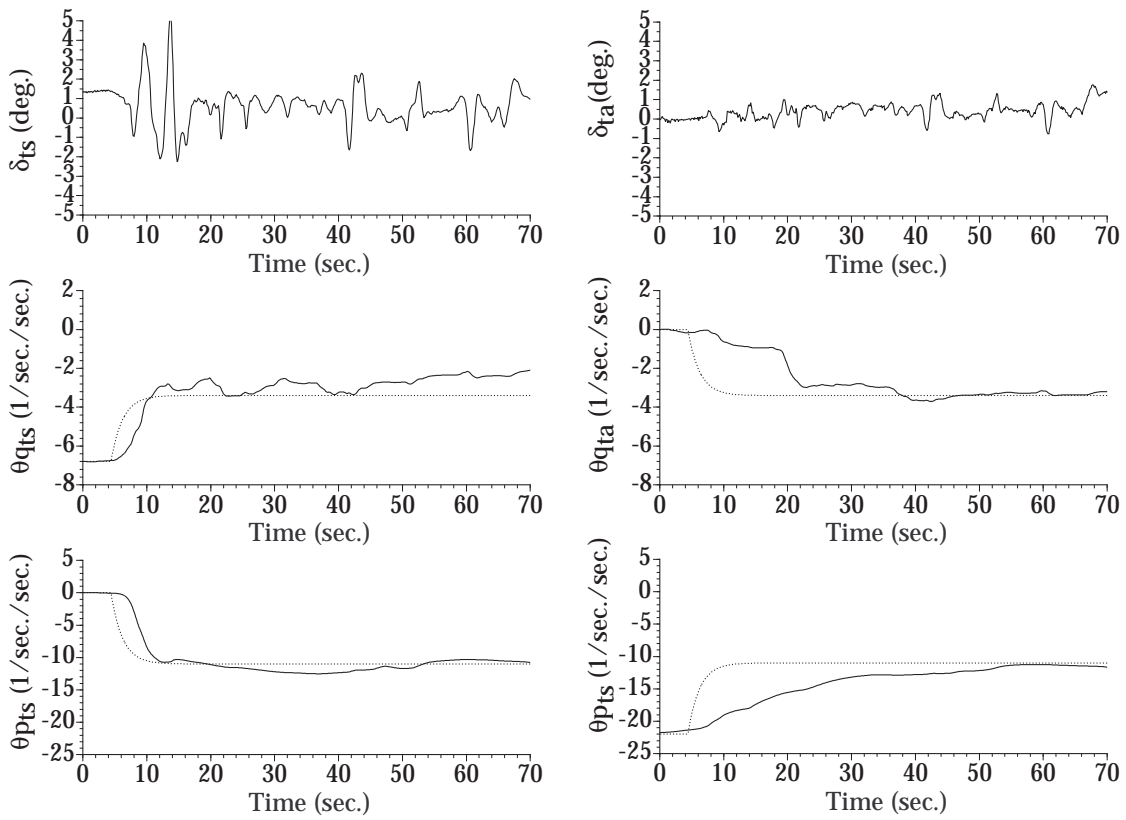


Figure 6: Elevon Control Derivatives from Flight Data

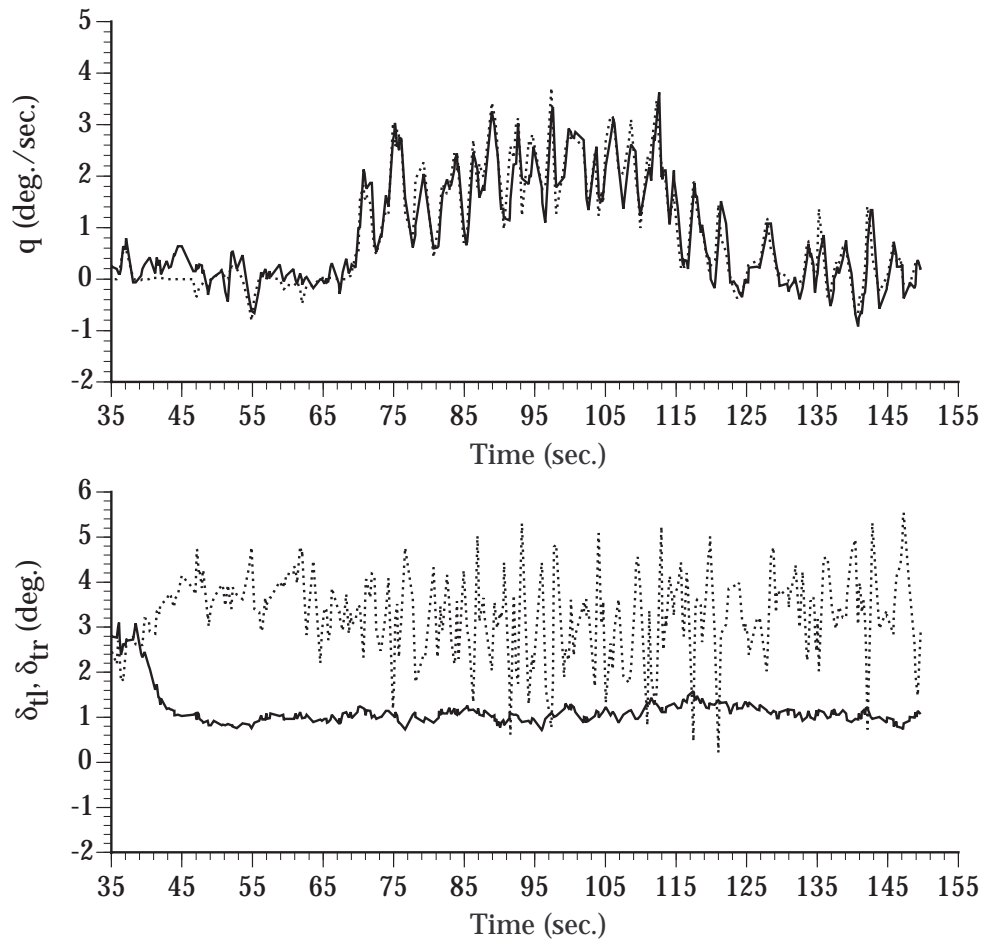


Figure 7: SDC Landing with Missing Left Elevon

Figure 1: Contribution of Nonlinear Effects to the \dot{q} Response

Figure 2: Contribution of Nonlinear Effects to the $\dot{\alpha}$ Response

Table 1: Longitudinal Stability and Control Derivatives

Figure 3: RLS Estimates of θ_{qts} and θ_{qta}

Figure 4: MSLS Estimates of θ_{qts} and θ_{qta}

Figure 5: VISTA F-16 Aircraft

Figure 6: Elevon Control Derivatives from Flight Data

Figure 7: SDC Landing with Missing Left Elevon